

# Excellence in Chemistry Research

## Announcing our new flagship journal

- Gold Open Access
- Publishing charges waived
- Preprints welcome
- Edited by active scientists



## Meet the Editors of *ChemistryEurope*



**Luisa De Cola**

Università degli Studi  
di Milano Statale, Italy



**Ive Hermans**

University of  
Wisconsin-Madison, USA



**Ken Tanaka**

Tokyo Institute of  
Technology, Japan



# Monitoring Conformation and Protonation States of Glutathione by Raman Optical Activity and Molecular Dynamics

Moumita Das,<sup>[a, b]</sup> Debraj Gangopadhyay,<sup>[a]</sup> Jana Hudecová,<sup>[c]</sup> Jiří Kessler,<sup>[a]</sup> Josef Kapitán,<sup>[c]</sup> and Petr Bour<sup>✉[a, b]</sup>

Glutathione (GSH) is a common antioxidant and its biological activity depends on the conformation and protonation state. We used molecular dynamics, Raman and Raman optical activity (ROA) spectroscopies to investigate GSH structural changes in a broad pH range. Factor analysis of the spectra provided protonation constants (2.05, 3.45, 8.62, 9.41) in good agreement with previously published values. Following the analysis, spectra of differently protonated forms were obtained by extrapolation. The complete deprotonation of the thiol group above pH 11 was clearly visible in the spectra; however, many spectral features did not change much with pH. Experimental spectra at

various pH values were decomposed into the simulated ones, which allowed us to study the conformer populations and quality of molecular dynamics (MD). According to this combined ROA/MD analysis conformation of the GSH backbone is affected by the pH changes only in a limited way. The combination of ROA with the computations thus has the potential to improve the MD force field and obtain more accurate populations of the conformer species. The methodology can be used for any molecule, but for a more detailed insight better computational techniques are needed in the future.

## Introduction

Glutathione (GSH,  $\gamma$ -Glu-Cys-Gly) tripeptide is sometimes referred to as the 'mother of all antioxidants'. Its presence in the human body has been linked to prevention of heart disease, dementia, autism, cancer, damage of the immune system, and neurodegeneration.<sup>[1]</sup> The reducing potential and the ability to capture free radicals come primarily from the thiol group.<sup>[2]</sup> The peptide is produced naturally, but stress factors, such as aging, toxins, infections, or radiation may result in lower GSH levels.

Oxidation of GSH leads to a dimer with the disulfide bridge.<sup>[3]</sup> While the stability in alkaline environment has not

been investigated so far, strongly acidic environment was suggested to induce formation of a five-membered thiazoline ring after a few days.<sup>[4]</sup> Raman signatures indicating a cyclization were seen previously for N-acetyl-L-cysteine after several hours both in acidic and alkaline media.<sup>[2d]</sup> Similar behavior of GSH, however, was not observed in the present study within the time of the experiments.

Apart from trying to better understand GSH behavior in a wide pH range of 1–12, we also use this molecule as a convenient system to broaden the application span of the Raman and ROA spectroscopies. These were found useful to monitor minor structural or conformational changes of smaller molecules under pH change.<sup>[5]</sup> However, GSH possesses more degrees of freedom and faithful simulations explaining experimental Raman and ROA spectra are quite challenging. The ROA technique had been previously applied to a wide range of organic molecules including nucleic acids,<sup>[6]</sup> sugars,<sup>[7]</sup> peptides,<sup>[8]</sup> and proteins.<sup>[9]</sup>

Although ROA spectra are more sensitive to the conformation than the Raman ones,<sup>[10]</sup> for large molecules it is difficult to decipher the spectral frequencies and intensities in terms of structural parameters. For example, while for the alanine dipeptide conformer populations could be obtained by a direct decomposition of experimental Raman and ROA spectra to the calculated shapes,<sup>[8d]</sup> precision of the simulations is usually too low to achieve this for more complex systems.<sup>[11]</sup> Flexible polar species are particularly challenging for the computational methods. We thus consider the GSH molecule also as a useful test of the combined experimental and computational Raman/ROA methodology. Molecular dynamics and the cluster-averaging techniques are used as they currently represent the most accurate computational tools for spectra simulations.<sup>[7a,12]</sup> Also

[a] M. Das, Dr. D. Gangopadhyay, Dr. J. Kessler, Prof. P. Bour  
Institute of Organic Chemistry and Biochemistry  
Czech Academy of Sciences  
Flemingovo náměstí 2  
16610 Prague 6 (Czech Republic)  
E-mail: bour@uochb.cas.cz

[b] M. Das, Prof. P. Bour  
Department of Analytical Chemistry  
Faculty of Chemical Engineering  
University of Chemistry and Technology  
Technická 5  
16628 Prague 6 (Czech Republic)

[c] Dr. J. Hudecová, Dr. J. Kapitán  
Department of Optics  
Palacký University  
17. listopadu 12  
77146 Olomouc (Czech Republic)

Supporting information for this article is available on the WWW under <https://doi.org/10.1002/cplu.202300219>

© 2023 The Authors. ChemPlusChem published by Wiley-VCH GmbH. This is an open access article under the terms of the Creative Commons Attribution Non-Commercial License, which permits use, distribution and reproduction in any medium, provided the original work is properly cited and is not used for commercial purposes.

for GSH they provided a reasonable basis for the spectra interpretation, structural and conformation predictions.

More specifically, in this work we investigated Raman and ROA spectra of several differently protonated GSH species (Figure 1). High quality experimental data were obtained, so that spectra of the pure forms could be extracted using factor analysis and extrapolation. Molecular dynamics simulations provided information on peptide geometry and flexibility, while the experimental spectra were interpreted on the basis of density functional theory. Finally, a decomposition of the experimental spectra into the simulated subspectra provided complementary information on molecular conformers and flexibility.

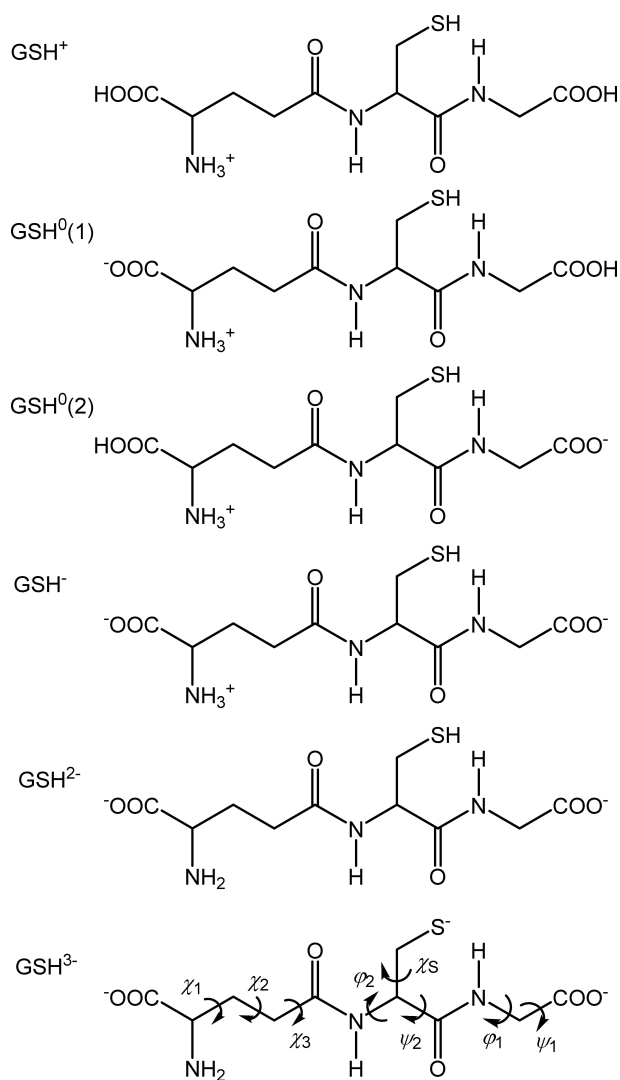


**Figure 1.** Investigated protonated forms of glutathione. The neutral species forms two isomers, GSH<sup>0</sup>(1) and GSH<sup>0</sup>(2). For GSH<sup>3-</sup> the main torsion angles are indicated.

## Results and Discussion

### Dependence of the Spectra on pH

Relative populations of the five protonated GSH forms and their spectra are plotted in Figure 2; in more detail the spectral changes under pH variation can be seen in Figures S1 and S2. The pK<sub>a</sub> constants of GSH obtained from the factor analysis (2.05, 3.45, 8.62, 9.41, Figure S3) are close to values published previously (2.13, 3.51, 8.74, 9.66).<sup>[13]</sup> For five pH values the populations are summarized in Table 1. The spectra of GSH<sup>+</sup>,

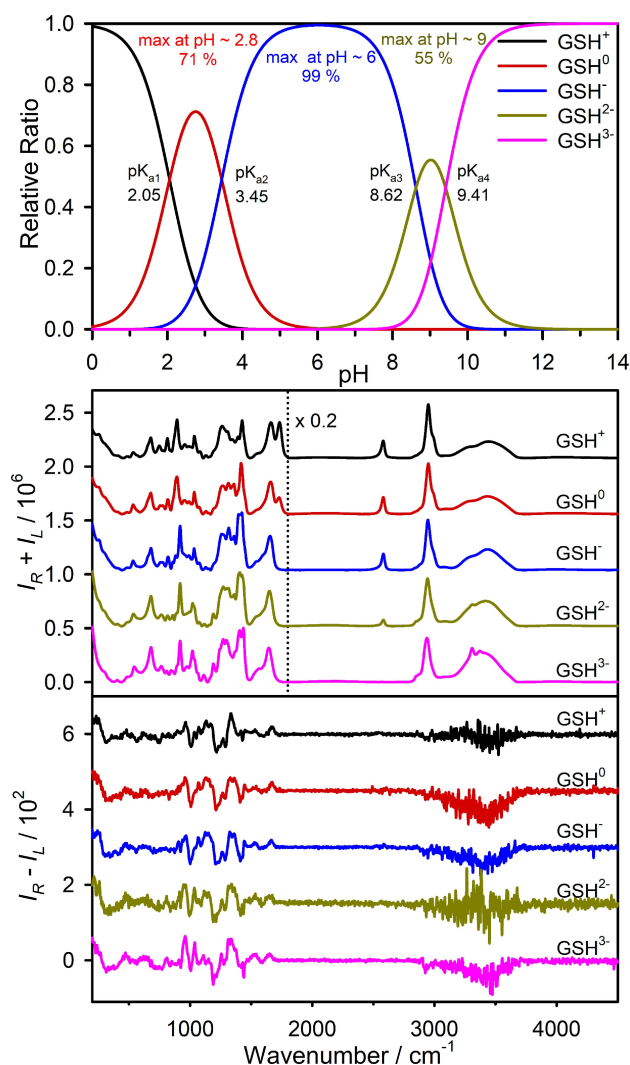


**Figure 2.** Relative ratios of five GSH forms as dependent on pH (top), their Raman ( $I_R + I_L$ , middle) and ROA ( $I_R - I_L$ , bottom) experimental spectra. Raman spectra above 1800  $\text{cm}^{-1}$  are multiplied by 0.2 for easier comparison.

**Table 1.** Relative populations of the GSH forms at selected pH values.

pH	GSH <sup>+</sup>	GSH <sup>0</sup>	GSH <sup>-</sup>	GSH <sup>2-</sup>	GSH <sup>3-</sup>
0.6	97%	3%	–	–	–
2.8	13%	71%	16%	–	–
6.3	–	–	99%	1%	–
9.1	–	–	18%	55%	27%
11.6	–	–	–	1%	99%

GSH<sup>-</sup>, and GSH<sup>3-</sup> could be obtained directly, as populations of these forms are close to 100% at pH 0.6, 6.3 and 11.6, respectively. Spectra of the remaining two forms were obtained by a combination of spectra measured at different pH:

$$S(\text{GSH}^{2-}) = (100 \times S_{9.1} - 18 \times S_{6.3} - 27 \times S_{11.6})/55,$$

$$S(\text{GSH}^0) = (100 \times S_{2.8} - 13 \times S_{0.6} - 16 \times S_{6.3})/71.$$

The titration experiments indicate that protonation/deprotonation of the thiol groups occurs mostly between pH 10 and 11, and the carboxyl groups are fully protonated below pH 3. As expected, bands most sensitive to the protonation originate in the affected groups, such as those of SH (~2571 cm<sup>-1</sup>) and carboxyl C=O (~1730 cm<sup>-1</sup>) stretching. Less sensitive are the bands within 800–900 cm<sup>-1</sup>, formed by CH<sub>2</sub> scissoring vibrations of the cysteine residue, C–C stretching and NH<sub>2</sub>/NH<sub>3</sub> bending. Raman shoulders around 2900 cm<sup>-1</sup>, slightly more pronounced at high pH, may perhaps be related to anharmonic effects.<sup>[14]</sup> At pH 11, NH<sub>2</sub> symmetric NH stretching mode generates a distinct sharp Raman band at 3310 cm<sup>-1</sup>, similarly as observed previously for the Ala–Ala dipeptide.<sup>[14a]</sup> Above 3000 cm<sup>-1</sup>, the ROA signal is not reliable due to the noise caused by a large scattering of water. More detailed band assignment can be found in Table S1.

Apart from the changes, Raman and ROA spectra also contain many features that are conserved across the entire pH range. For example, signals stemming from the backbone (e.g., C–C stretching around 1000 cm<sup>-1</sup>, CH bending around 1300 cm<sup>-1</sup>, amide I at 1650 cm<sup>-1</sup>) provide similar ROA patterns. In Figure S2, where the spectra are plotted in a broader range of wave-

numbers (~45–4500 cm<sup>-1</sup>), for all pHs we see negative ROA close to the spectrometer limit of ~45 cm<sup>-1</sup>. It quickly develops in a positive band around 95 cm<sup>-1</sup>. The relative intensities of the low-frequency ROA signal is quite large, similarly as observed previously for some polypeptides,<sup>[21b]</sup> proteins,<sup>[9d]</sup> or chiral liquids.<sup>[15]</sup> These many conservative ROA features suggest that the GSH conformation is not radically changed under the pH variation.

### GSH Conformations from Molecular Dynamics

The relative independence of the spectra of the protonation state is consistent with the molecular dynamics (MD) simulations, also indicating only minor differences in the structure. The probability histograms of the principal torsion angles do not change dramatically with the protonation (Figure 3, left). Angle  $\varphi_1$  is relatively freely rotating, sampling the favorite positions at ~60, -60 and 180°,  $\psi_1$  at the terminus reacts on the carboxyl protonation,  $\varphi_2$  and  $\psi_2$  distributions in GSH<sup>3-</sup> differ a lot from the other forms because of the deprotonation of the close SH group. The angles  $\chi_1$ ,  $\chi_2$  and  $\chi_3$  in the glutamate part are not so much affected by pH, neither is  $\chi_p$  determining position of the sulfur to the rest of the molecule. We can see these differences also in the dependencies of MD free energies on  $\varphi_2$  and  $\psi_2$  plotted in Figure 3, right, recalculated from the conformer populations. Other angle combinations are displayed in Figure S4. From these analyses it appears that the GSH<sup>3-</sup> form differs most from the others in terms of the peptide backbone conformation, which can also be viewed as a stabilizing effect of the SH group on the structure. The otherwise limited effect of the protonation on GSH backbone

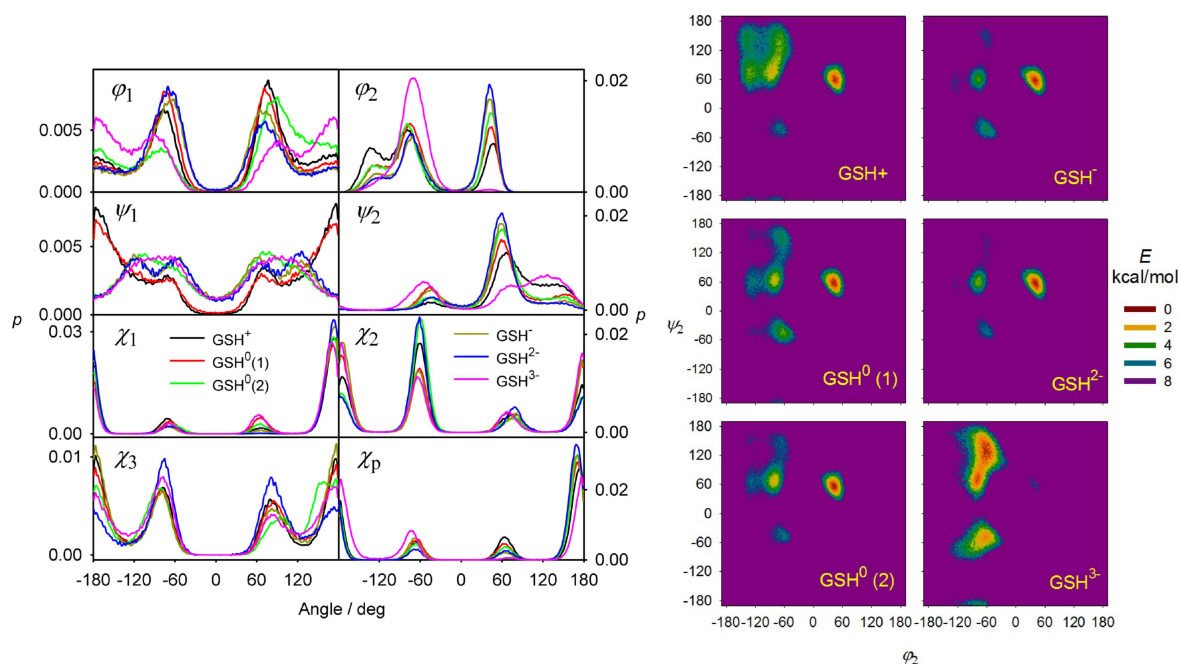


**Figure 3.** MD results: (left) probability distributions of characteristic torsion angles, for the six GSH protonated forms, and (right) dependence of the free energy on the  $\varphi_2$  and  $\psi_2$  torsion angles.

structure can be in general related to the theory of electrolytes<sup>[16]</sup> and water polarity, where the environment damps interactions among the partial atomic charges of GSH.

The MD results are in a rough agreement with previous NMR and computational studies.<sup>[17]</sup> For example, with the Gromacs force field and molecular dynamics coupled with NMR data, similar angular distributions were found to those in Figure 3.<sup>[17d]</sup> the molecule was found quite flexible, and rather minor differences were observed between differently charged GSH forms. However, the free dynamics with the Amber force field used in the present study predicts slightly different conformer ratios.

Crystal data on glutathione structure are mostly available for the deprotonated ( $\text{GSH}^-$ ) or neutral ( $\text{GSH}^0$ ) forms, also in complexes with functional proteins. The crystals are not much relevant for the solution studies, but they confirm that the molecule is quite flexible as predicted by MD. Indeed, all torsion angles can adopt a range of values in the crystals and complexes, depending on the environment.<sup>[18]</sup>

**Spectra Modeling.** The calculated Raman and ROA spectra reasonably well agree with the experimental ones (Figure 4). Almost band-to-band agreement is achieved for Raman; however, discrepancies occur below  $800\text{ cm}^{-1}$  where vibrations involving the sulfur atom significantly participate. It is also almost impossible to subtract accurately the fluorescent background from experimental spectra in this region. Another source of error may be the MD force field, as it was not

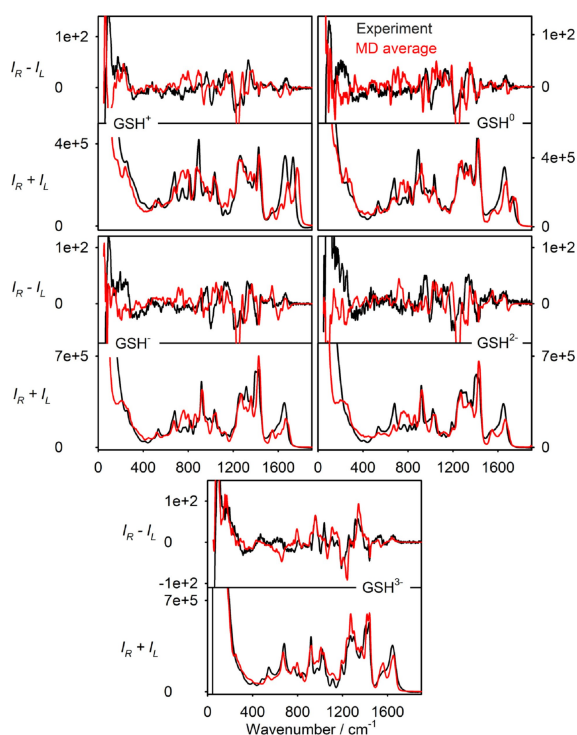


**Figure 4.** Calculated (red) and experimental (black) Raman and ROA spectra of five GSH forms. The calculated spectra were normalized (one y-factor for all) to reproduce average Raman integral intensity within  $400\text{--}1800\text{ cm}^{-1}$  and x-scaled by 0.98. Experimental Raman baseline was arbitrarily corrected by a 5<sup>th</sup> order polynomial, idealized experimental spectra are shown for  $\text{GSH}^0$  and  $\text{GSH}^{2-}$ .

particularly optimized for heavier atoms such as sulfur.<sup>[19]</sup> Sulfur also has a relatively complicated electronic structure, sometimes problematic for DFT.<sup>[20]</sup> The wavenumber-scaling factor of 0.98 shifted most of the calculated bands closer to the experimental positions, but visible deviations remain for the C=O stretching bands within  $1600\text{--}1800\text{ cm}^{-1}$ . These would have required an extra scaling factor of 0.96, which we find superfluous just for the sake of visual comparison. Most of the ROA bands are also reproduced correctly in terms of the signs and relative intensities, albeit with much larger error than for Raman. At the lowest wavenumber region ( $\sim <400\text{ cm}^{-1}$ ) the experimental ROA spectra may be distorted due to the fluorescent background.

To illustrate the effect of the force field, in Figure 5, left, the ROA and Raman spectra of  $\text{GSH}^{3-}$  as generated with the GAFF and Amber force fields are compared to each other and the experiment. Both force fields reproduce the experimental data reasonably well, with some inaccuracies. For the Raman spectrum, Amber reproduces better the fine splitting around  $763\text{ cm}^{-1}$ , and the  $917/1020$  and  $1405/1436\text{ cm}^{-1}$  bands. The region around  $1271\text{ cm}^{-1}$  and the relative strength of the  $1560/1643\text{ cm}^{-1}$  bands are better reproduced by GAFF. For ROA, Amber seems to be more apt to reproduce peak intensities at  $1310$ ,  $1409$ ,  $1525$  and  $1659\text{ cm}^{-1}$ , while the  $1038\text{ cm}^{-1}$  positive band is better reproduced by GAFF, etc. Interestingly, the huge positive low-frequency ( $50\text{--}300\text{ cm}^{-1}$ ) ROA signal is at least qualitatively reproduced by both simulations. The low-frequency ROA may reflect both motions of the peptide as well as its interactions with the solvent.<sup>[14b,15,21]</sup>

Also the choice of the solvent model has a significant effect on the spectra. The explicit involvement of the water molecules in the clusters appeared very beneficial for the resultant spectral shape, while when the spectra were simulated for GSH with the polarizable continuum model (CPCM) only, resultant ROA and Raman curves were less realistic (Figure 5, right). This can be

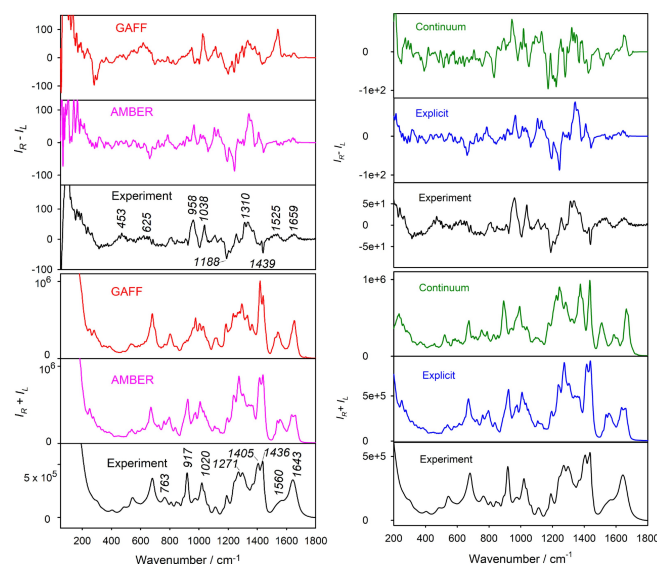


**Figure 5.**  $\text{GSH}^{3-}$  ROA and Raman spectra calculated (left) with the GAFF and AMBER force fields, and (right) with the CPCM continuum and explicit solvent models, and the experiment.

related to directional hydrogen bonds, not adequately described by CPCM.<sup>[22]</sup>

To further explore stability of the results with respect to the simulation parameters, for  $\text{GSH}^{3-}$  we investigated the effect of the number of averaged MD clusters on the calculated spectra. As an example, 100 and 1000 cluster averages are compared to the experiment in Figure S5. For the Raman spectra the more extensive averaging led to almost no change. Bigger differences appear for ROA, where the 1000 cluster average gives a smoother spectrum, however, without a significant change of the principal trends. The greater ROA sensitivity to computational parameters is consistent with previous reports, where more clusters were recommended for ROA simulations than for Raman.<sup>[23]</sup>

Special attention had to be paid to the  $\text{GSH}^0$ , where the deprotonation can occur either on the side chain [ $\text{GSH}^0(1)$ ] or peptide main chain [ $\text{GSH}^0(2)$ ]. We simulated the experiment by 1:1 mixing of these sub-forms. Indeed, the mixture provides Raman spectrum in a few aspects closer to the experiment than any of the components (Figure S6). Unfortunately, it is not possible to determine the ratio more accurately, due to the limited precision of the simulations. The bigger differences in the Raman spectra compared to ROA are rather unusual; in most cases the opposite is true.<sup>[8a,c,10]</sup> For  $\text{GSH}$ , however, the protonation occurs at the locally achiral carboxyl groups, not much contributing to ROA signal.

### Experimental vs. MD conformer populations

We chose the main conformers according to  $\psi_2$  and  $\chi_3$ . These torsion angles are close to the molecular center, and significantly affect molecular shape. The assignment of the six conformers to the potential energy minima for  $\text{GSH}^{3-}$  is shown in Figure 6. For all forms except  $\text{GSH}^0$  arbitrary energy surfaces and conformer probabilities as functions of  $\psi_2$  and  $\chi_3$  were calculated, using the decomposition of the experimental spectra into the calculated spectra of 1000 MD snapshots. Relative populations of conformers 1–6 were calculated from MD probabilities (Figure S4) by integration, using the limits in Table 2. The populations are compared to those obtained by the spectra analysis in Table 3.

For Raman, we suppose that the populations obtained from the spectra bear a larger error than for ROA, due to the similarity of the spectra of different form. Nevertheless, both spectral values in general follow the MD results, with the exception of  $\text{GSH}^+$  where the ROA spectral decomposition predicts 2% of conformer 6, while it is 45% from MD. Smaller, but still relatively important inconsistencies occur also for the other forms. For example, for the 3<sup>rd</sup> conformer of  $\text{GSH}^{2-}$  27% and 3% are respectively predicted by ROA and MD.

The dependencies of the free energy on the  $\psi_2$  and  $\chi_3$  torsion angles obtained by the spectral fit and MD are plotted in Figure 7, top, the resultant fitted spectra are plotted at the bottom. Note that the fitted energy surfaces, although they should converge to the true dependencies,<sup>[24]</sup> are for a limited coverage of the  $(\psi_2, \chi_3)$  plane by the MD snapshots just arbitrary

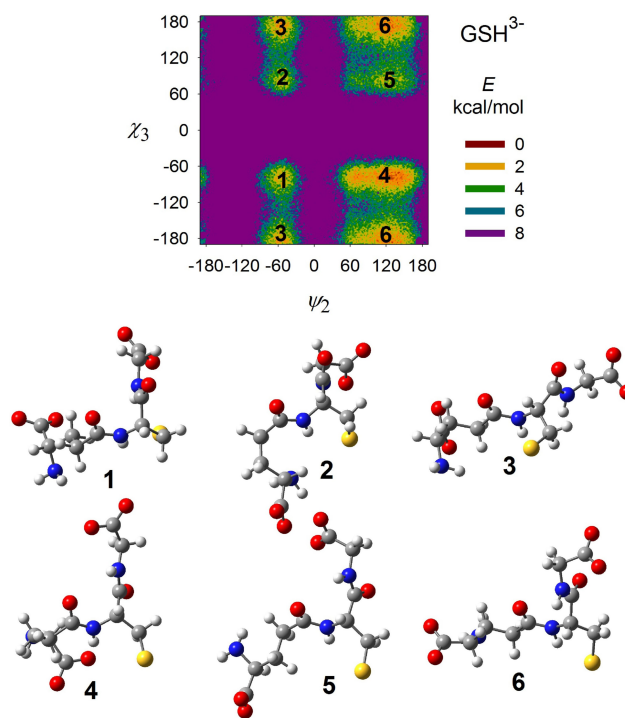


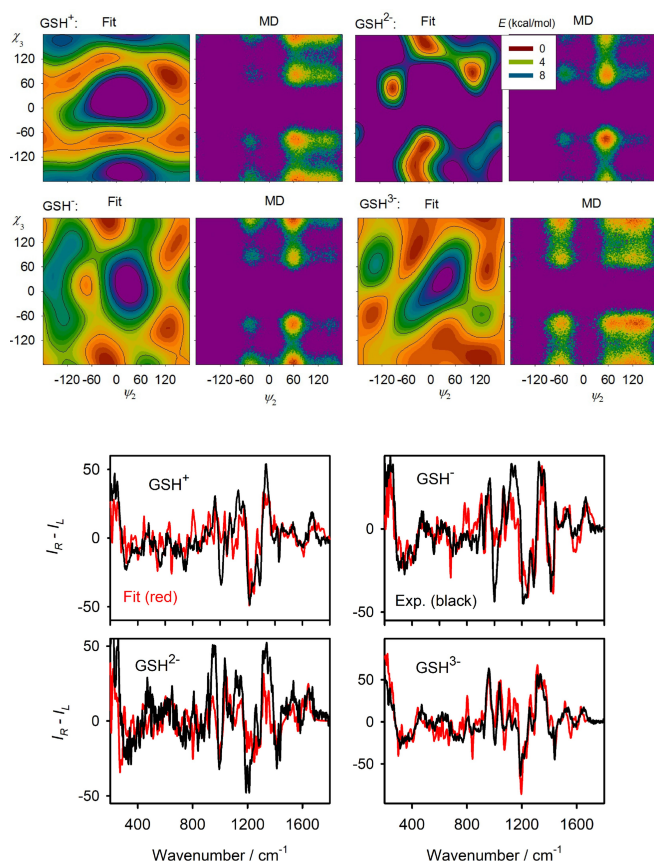
Figure 6.  $\text{GSH}^{3-}$ , dependence of the free energy of on the  $\psi_2$  and  $\chi_3$  torsion angles, and example snapshot geometries representing the six conformer classes.

Table 2. Ranges of  $\psi_2$  and  $\chi_3$  in the six conformers.

Conformer	$\psi_2/\text{deg.}$	$\chi_3/\text{deg.}$
1	(-120, 0)	(-120, 0)
2	(-120, 0)	(0, 125)
3	(-120, 0)	outside (-120, 125)
4	outside (-120, 0)	(-120, 0)
5	outside (-120, 0)	(0, 125)
6	outside (-120, 0)	outside (-120, 125)

Table 3. Relative conformer populations (%) from MD and from the Raman/ROA spectra decomposition.

Conformer:	1	2	3	4	5	6
$\text{GSH}^+$ :						
Raman	37	0	0	4	1	58
ROA	10	11	2	34	41	2
MD	2	1	4	26	22	45
$\text{GSH}^0$ :						
MD	6	3	7	23	19	42
$\text{GSH}^{2-}$ :						
Raman	12	8	25	30	1	24
ROA	4	4	31	20	13	28
MD	3	3	12	22	18	42
$\text{GSH}^{2-}$ :						
Raman	12	8	36	22	1	21
ROA	3	9	27	14	14	33
MD	3	5	3	33	29	27
$\text{GSH}^{3-}$ :						
Raman	8	6	17	26	8	35
ROA	2	11	14	18	12	43
MD	8	7	14	26	13	32



**Figure 7.** (Top) potential energies as functions of ( $\psi_2, \chi_3$ , in degrees) obtained by the fit of experimental ROA spectra with 1000 MD snapshot spectra, and from free MD (100000 snapshots, 1  $\mu$ s run). (Bottom) the experimental ROA spectra and the fit.

functions mediating the fit.<sup>[25]</sup> Yet some relations to the MD results are apparent, e.g., for  $\text{GSH}^+$  the fit suggests that the most favorite position is close to conformer 5 ( $\psi_2, \chi_3 \sim (140^\circ, 75^\circ)$ ) while conformers 3 and 6 with  $\chi_3 \sim 180^\circ$  are not present in the sample, etc.

The spectral decompositions indicate inaccuracies in the force field, but they are themselves affected by the DFT error and other approximations, and about 10–20% uncertainty in the conformer populations thus obtained can be expected.<sup>[8d,23,25]</sup> An error about 10% can also be estimated for  $\text{GSH}^{3-}$  from the conformer populations obtained from various numbers of averaged clusters (Figure S7, other forms provided similar dependencies). Also, the division into the 2D conformer classes is rather arbitrary; in principle, multi-dimensional conformer and spectra analysis is possible, but this would require unreasonable amount of MD snapshots and computer effort. In spite of these constraints, we believe that the combined computational and spectral analysis of GSH behavior under pH variations well documents limitations, current possibilities and also future potential of the method for biomolecular studies.

## Conclusions

We measured glutathione Raman and ROA spectra in a broad pH interval, to investigate the behavior of this molecule, and to explore potential of the combined spectroscopic and computational methodology for biomolecular structural studies. Various protonation states of the molecule provided readily recognizable changes in the spectra. Using the factor analysis of Raman intensities, we could extract experimental protonation constants that were consistent with the previous works. We then could use the data about fractions of the protonated species to obtain Raman and ROA spectra of five pure peptide forms ( $\text{GSH}^+$ ,  $\text{GSH}^0$ ,  $\text{GSH}^-$ ,  $\text{GSH}^{2-}$ ,  $\text{GSH}^{3-}$ ), either directly or by extrapolation.

Except for the changes caused by the protonation, spectral intensities in many aspects remained unchanged and indicated that pH has a limited effect on conformational behavior of the molecule. This was consistent with the molecular dynamics simulations. The MD and spectroscopic data could be mutually verified by comparison of the simulated and experimental spectra. GSH geometries were also divided into six conformer classes, based on the central  $\psi_2$  and  $\chi_3$  angles, and the experimental spectra were decomposed into calculated sub-spectra, which revealed experimental conformer ratios, roughly in agreement with the MD results. The combined Raman/ROA/computational methodology appears useful for monitoring and controlling of properties of biologically-active molecules in solutions.

## Experimental Section

### Spectroscopy

Commercial glutathione peptide (Sigma-Aldrich G6529, purity > 98%), deionized water (Purcellab flex, 18.2 M $\Omega$ .cm), NaOH (Sigma-Aldrich S2770) and HCl (Sigma-Aldrich H9892) were used. pH was regulated by 1 M HCl and 1 M NaOH maintaining the same 0.5 M concentration of GSH. Within pH 1 and pH 12 Raman spectra were accumulated for 180 min on an OceanOptics QEPro spectrometer using the 785 nm excitation, pH was measured by an indicator paper. For control, HCl was added stepwise to the pH 12 solution to achieve lower pH values, which led to the same relative Raman intensities as when given pH was constant from the beginning (Figure S1).

No protective measures were taken against sample oxidation, but the sample stability was also monitored by the electron spray ionization mass spectroscopy and  $^1\text{H}$  and  $^{13}\text{C}$  NMR spectra, which did not reveal any undesired changes within the timescale of our experiments. Neither Raman spectra indicate a significantly decay of the sample during the ROA accumulation (Figure S8).

Further measurements were done on a custom-made spectrometer<sup>[14b]</sup> working with the 532 nm excitation and simultaneously recording Raman and ROA spectra. In this case pH was measured with a Thermo Orion<sup>™</sup> microglass electrode. The samples were held in a rectangular fused silica cell (3  $\times$  4 mm, 80  $\mu$ l volume) at temperature 20  $^\circ\text{C}$ , laser power at the sample was about 340 mW.

For fine titration series 21 samples with pH from 0.6 to 12.7 were prepared by mixing of two solutions: 0.4 M GSH dissolved in 1 M NaOH (pH 12.7) and 0.4 M GSH dissolved in 0.5 M HCl (pH 0.6). Final solutions were passed through a PVDF filter with 0.2  $\mu\text{m}$  pore size and Raman spectra were measured for 10 minutes. Spectrum of pure water was subtracted (within pH 1–11 it is practically indistinguishable from HCl/NaOH solutions<sup>[26]</sup>) and residual background further eliminated by an asymmetric-least-squares smoothing.<sup>[27]</sup>

ROA spectra were measured at pH 0.6, 2.8, 6.3, 9.1, and 11.6, using 0.3 M GSH concentration and 34 h accumulation. The five pH values were chosen to maximize fraction of each protonated form. Signal of aqueous HCl and NaOH solutions of corresponding pH was subtracted from the corresponding Raman spectra. Raman and ROA experimental intensities are presented in  $\text{cm} \cdot \text{J}^{-1}$  (electron count per wavenumber interval per irradiation energy).

### Factor Analysis

A factor analysis<sup>[28]</sup> of these experiments was used to obtain Raman spectra of the five GSH forms from Figure 1. Briefly, each spectrum  $Y_i(\nu)$  was considered as a sum [Eq. (1)]:

$$Y_i(\nu) = \sum_{j=1}^M w_j v_{ij} S_j(\nu) \quad (1)$$

where  $w_j$  are weights,  $S_j(\nu)$  are normalized subspectra, and  $v_{ij}$  are scores forming a unitary matrix. The number of original spectra ( $N=21$ ) was reduced to a basis of  $M=5$  subspectra. The protonation constants  $pK_a$  were found by a fitting procedure,<sup>[26]</sup> using the Henderson-Hasselbalch equation [Eq. (2)]

$$pH = pK_a + \log([A^-]/[HA]) \quad (2)$$

to relate equilibrium concentrations of variously deprotonated  $[A^-]$  and protonated  $[HA]$  forms. The analysis included spectral region within 200–3150  $\text{cm}^{-1}$  where the measurement is most reliable. In particular, it is difficult to subtract the background outside this interval.

Similar analysis could not be done for ROA, where the spectra are noisier and the accumulation times much longer. ROA spectra of pure protonated forms could be obtained using the knowledge about the protonation constants and an extrapolation as specified above.

### Computations

Initial GSH geometries were optimized by energy minimization in the Gaussian 16 software<sup>[29]</sup> using the B3LYP<sup>[30]</sup> functional, 6-311 + +G(d,p) basis set, and CPCM water model. The atomic charges thus obtained were used in a fitting procedure<sup>[31]</sup> providing force field for Amber MD programs.<sup>[32]</sup> Within Amber, the peptide was placed into a cubic water box (40 Å a side, 2141 water molecules), and according to the protonation state,  $\text{Na}^+$  and  $\text{Cl}^-$  counterions were added to keep system neutrality. The dynamics were performed at 300 K using NVT ensemble, GAFF<sup>[19]</sup> or Amber<sup>[33]</sup> force fields, and 1 fs integration time step. As the Amber force field provided slightly more realistic spectra, the Amber results are reported if not indicated otherwise. After an equilibration, 1000 snapshots for spectra calculations were extracted in 1 ns intervals. A larger number of snapshots (100000) was used for MD trajectory analysis.

From the snapshots, peptide-water clusters were made, leaving only water molecules hydrogen-bonded and closer than 2.6 Å to the peptide. Also the  $\text{Na}^+$  and  $\text{Cl}^-$  counterions were deleted as their effect on the resultant spectra was quite minor. The cluster geometries were partially optimized in the normal mode vibrational coordinates,<sup>[34]</sup> using the Gaussian and Qgrad<sup>[35]</sup> programs, and the B3LYP/6-311 + +G(d,p)/CPCM level of approximation. On water atoms, smaller 6-31G basis set was used. For the clusters, vibrational frequencies and backscattering Raman and SCP<sup>[10]</sup> ROA intensities were calculated at the same level as the optimized geometry and averaged. For smooth spectra, the frequencies were scaled by 0.98 and the intensities convoluted with Lorentzian bands 10  $\text{cm}^{-1}$ .

### Spectral Decomposition and Fitting

To relate the spectra to the conformation of GSH backbone decomposition algorithm based on arbitrary potential energy surfaces was used.<sup>[24,25]</sup> Briefly, the experimental spectra  $S_e$  were thought of as weighted sums of the calculated ones  $S_c$ , shown in Equation (3):

$$S_e \approx \sum_{i=1}^N p_i S_{c,i} \quad (3)$$

The error  $\delta = \int (S_e - \sum c_i S_{c,i})^2 d\nu$  was considered as a function of associated energies  $e_i$  since  $p_i = \exp(-e_i/kT)$ , where  $kT$  is the Boltzmann temperature quantum. The energies were expanded to plane wave (cos/sin) basis functions  $g_k$ ,

$$e_i = \sum_{k=1}^M d_k g_k(x_i),$$

where  $x_i$  stands for selected coordinate/coordinates. Note that even for a large number of snapshots/calculated spectra ( $N \sim 1000$ ), the number of the parameters  $d_k$  to be optimized remains restricted (we chose  $M=25$ ). For the decomposition the calculated frequencies were scaled to match the strongest Raman bands exactly and other frequencies between were interpolated. Although the algorithm can be applied more generally, we restricted ourselves to conformers differing by two of the torsion angles, used as the reference coordinates  $x_i$ .

### Acknowledgements

The work was supported by the Grant Agency (22-04669S) and Ministry of Education (e-INFRA CZ 90254) of the Czech Republic.

### Conflict of Interests

*JK and JH pursue commercialization of the ROA spectrometer as employees of Palacký University Olomouc in cooperation with ZEBR and Meopta - optika companies. The other authors declare no conflict of interest.*

### Data Availability Statement

The data that support the findings of this study are available in the supplementary material of this article.

**Keywords:** density functional theory · glutathione · molecular dynamics · Raman optical activity · spectra modeling

- [1] a) T. Ziglari, A. Allameh, *Aflatoxins – Recent Advances and Future Prospects* (Ed.: M. Razzaghi-Abyaneh), IntechOpen, Iran **2013**, pp. 267–286; b) S. L. Nuttall, U. Martin, A. J. Sinclair, M. J. Kendall, *Lancet* **1998**, 351, 645–645; c) S. C. De Rosa, M. D. Zaretsky, J. G. Dubs, M. Roederer, M. Anderson, A. Green, D. Mitra, N. Watanabe, H. Nakamura, I. Tjioe, *Eur. J. Clin. Invest.* **2000**, 30, 915–929; d) R. L. Woltjer, W. Nghiem, I. Maezawa, D. Milatovic, T. Vaisar, K. S. Montine, T. J. Montine, *J. Neurochem.* **2005**, 93, 1047–1056; e) Z. Ke, Z. Yu, Q. Huang, *Plasma Processes Polym.* **2013**, 10, 181–188.
- [2] a) H. J. Forman, H. Zhang, A. Rinna, *Mol. Aspects Med.* **2009**, 30, 1–12; b) G. M. A. Cançado, V. E. De Rosa, J. H. Fernandez, L. G. Maron, R. A. Jorge, M. Menossi, *Funct. Plant Biol.* **2005**, 32, 1045–1055; c) C. H. Foyer, H. Lopez-Delgado, J. F. Dat, I. M. Scott, *Physiol. Plant.* **1997**, 100, 241–254; d) D. Gangopadhyay, M. Das, K. K. Singh, P. Sharma, R. K. Singh, P. Tandon, *J. Phys. Chem. B* **2018**, 122, 10306–10314; e) P. Moldéus, I. A. Cotgreave, *Methods Enzymol.* **1994**, 234, 482–492; f) L. Sjöberg, T. E. Eriksen, L. Revesz, *Radiat. Res.* **1982**, 89, 255–263; g) S. P. Mezyk, *J. Phys. Chem.* **1996**, 100, 8861–8866.
- [3] a) D. P. Dixon, I. Cummins, D. J. Cole, R. Edwards, *Curr. Opin. Plant Biol.* **1998**, 1, 258–266; b) M. Tamba, A. Torreggiani, *Res. Chem. Intermed.* **2002**, 28, 57–70.
- [4] R. B. Martin, S. Lowey, E. L. Elson, J. T. Edsall, *J. Am. Chem. Soc.* **1959**, 81, 5089–5095.
- [5] a) J. Hudecová, J. Kapitán, M. Dračinský, P. Michal, V. Profant, P. Bouř, *Chem. Eur. J.* **2022**, 28, e202202045; b) D. Gangopadhyay, P. Sharma, S. K. Singh, P. Singh, N. Tarcea, V. Deckert, J. Popp, R. K. Singh, *Chem. Phys. Lett.* **2015**, 618, 225–230; c) P. Sharma, D. Gangopadhyay, P. Singh, P. C. Mishra, V. Deckert, J. Popp, R. K. Singh, *Chem. Phys. Lett.* **2014**, 613, 127–132; d) D. Gangopadhyay, P. Sharma, R. Nandi, M. Das, S. Ghosh, R. K. Singh, *RSC Adv.* **2016**, 6, 112562–112567; e) D. Gangopadhyay, P. Sharma, S. K. Singh, P. Singh, V. Deckert, J. Popp, R. K. Singh, *RSC Adv.* **2016**, 6, 58943–58949.
- [6] E. W. Blanch, L. Hecht, L. D. Barron, *Methods* **2003**, 29, 196–209.
- [7] a) J. R. Cheeseman, M. S. Shaik, P. L. A. Popelier, E. W. Blanch, *J. Am. Chem. Soc.* **2011**, 133, 4991–4997; b) Z. Q. Wen, L. D. Barron, L. Hecht, *J. Am. Chem. Soc.* **1993**, 115, 285–292; c) V. Palivec, V. Kopecký, P. Jungwirth, P. Bouř, J. Kaminský, H. Martinez-Seara, *Phys. Chem. Chem. Phys.* **2020**, 22, 1983–1993.
- [8] a) S. Yamamoto, M. Straka, H. Watarai, P. Bouř, *Phys. Chem. Chem. Phys.* **2010**, 12, 11021–11032; b) K. J. Jalkanen, R. M. Nieminen, M. Knapp-Mohammady, S. Suhai, *Int. J. Quantum Chem.* **2003**, 92, 239–259; c) A. S. Perera, J. Cheramy, C. Merten, J. Thomas, Y. J. Xu, *ChemPhysChem* **2018**, 19, 2234–2242; d) J. Jungwirth, J. Šebestík, M. Šafařík, J. Kapitán, P. Bouř, *J. Phys. Chem. B* **2017**, 121, 8956–8964.
- [9] a) S. Lubner, M. Reiher, *J. Phys. Chem. B* **2010**, 114, 1057–1063; b) C. Mensch, C. Johannessen, *ChemPhysChem* **2018**, 19, 3134–3143; c) I. H. McColl, E. W. Blanch, L. Hecht, L. D. Barron, *J. Am. Chem. Soc.* **2004**, 126, 8181–8188; d) J. Kessler, J. Kapitán, P. Bouř, *J. Phys. Chem. Lett.* **2015**, 6, 3314–3319; e) V. Parčhaňský, J. Kapitán, P. Bouř, *RSC Adv.* **2014**, 4, 57125–57136.
- [10] L. Nafie, *Vibrational optical activity: Principles and applications*, Wiley, Chichester **2011**.
- [11] a) X. Li, K. H. Hopmann, J. Hudecová, W. Stensen, J. Novotná, M. Urbanová, J. S. Svendsen, P. Bouř, K. Ruud, *J. Phys. Chem. A* **2012**, 116, 2554–2563; b) K. H. Hopmann, J. Šebestík, J. Novotná, W. Stensen, M. Urbanová, J. Svendsen, J. S. Svendsen, P. Bouř, K. Ruud, *J. Org. Chem.* **2012**, 77, 858–869.
- [12] a) P. Bouř, V. Sychrovský, P. Maloň, J. Hanzlíková, V. Baumruk, J. Pospíšek, M. Buděšínský, *J. Phys. Chem. A* **2002**, 106, 7321–7327; b) S. Yamamoto, J. Kaminský, P. Bouř, *Anal. Chem.* **2012**, 84, 2440–2451; c) J. R. Cheeseman, M. J. Frisch, *J. Chem. Theory Comput.* **2011**, 7, 3323–3334; d) L. N. Vidal, F. Egidi, V. Barone, C. Cappelli, *J. Chem. Phys.* **2015**, 142, 174101.
- [13] A. Krezel, W. Bal, *Bioinorg. Chem. Appl.* **2004**, 2, 293–305.
- [14] a) M. Hope, J. Šebestík, J. Kapitán, P. Bouř, *J. Phys. Chem. A* **2020**, 124, 674–683; b) P. Michal, R. Čelechovský, M. Dudka, J. Kapitán, M. Vůjtek, M. Berešová, J. Šebestík, K. Thangavel, P. Bouř, *J. Phys. Chem. B* **2019**, 123, 2147–2156.
- [15] P. Michal, J. Kapitán, J. Kessler, P. Bouř, *Phys. Chem. Chem. Phys.* **2022**, 24, 19722–19733.
- [16] J. L. Liu, C. L. Li, *AIP Adv.* **2019**, 9, 015214.
- [17] a) M. J. York, G. R. Beilharz, P. W. Kuchel, *Int. J. Pept. Protein Res.* **1987**, 29, 638–646; b) S. Fujiwara, G. Formicka-Kozłowska, H. Kozłowski, *Bull. Chem. Soc. Jpn.* **1977**, 50, 3131–3135; c) D. L. Rabenstein, *J. Am. Chem. Soc.* **1973**, 95, 2797–2803; d) O. Lampela, A. H. Juffer, A. Rauk, *J. Phys. Chem. A* **2003**, 107, 9208–9220; e) R. Zhang, W. Wu, *J. Mol. Liq.* **2011**, 162, 20–25.
- [18] a) W. Wright, *Acta Crystallogr.* **1958**, 11, 632–642; b) L. Prade, R. Huber, T. H. Manoharan, W. E. Fahl, W. Reuter, *Structure* **1997**, 5, 1287–1295; c) H. Nishimasa, R. Ishitani, K. Yamashita, C. Iwashita, A. Hirata, H. Hori, O. Nureki, *Proc. Natl. Acad. Sci. USA* **2009**, 106, 8180–8185.
- [19] J. Wang, R. M. Wolf, J. W. Caldwell, P. A. Kollman, D. A. Case, *J. Comput. Chem.* **2004**, 25, 1157–1174.
- [20] W. M. Holden, E. P. Jahrman, N. Govind, J. T. Seidler, *J. Phys. Chem. A* **2020**, 124, 5415–5434.
- [21] a) J. Kapitán, V. Baumruk, V. Kopecký Jr, R. Pohl, P. Bouř, *J. Am. Chem. Soc.* **2006**, 128, 13451–13462; b) S. Yamamoto, S. Ishiro, J. Kessler, P. Bouř, *Phys. Chem. Chem. Phys.* **2021**, 23, 26501–26509.
- [22] P. Bouř, D. Michalík, J. Kapitán, *J. Chem. Phys.* **2005**, 122, 144501.
- [23] K. H. Hopmann, K. Ruud, M. Pecul, A. Kudelski, M. Dračinský, P. Bouř, *J. Phys. Chem. B* **2011**, 115, 4128–4137.
- [24] V. Parčhaňský, J. Kapitán, J. Kaminský, J. Šebestík, P. Bouř, *J. Phys. Chem. Lett.* **2013**, 4, 2763–2768.
- [25] V. Schrenková, M. S. Para Kkadan, J. Kessler, J. Kapitán, P. Bouř, *Phys. Chem. Chem. Phys.* **2023**, 25, 8198–8208.
- [26] J. Palacký, P. Mojžeš, J. Bok, *J. Raman Spectrosc.* **2011**, 42, 1528–1539.
- [27] P. Eilers, H. Boelens, *Leiden University Medical Centre report* **2005**.
- [28] E. R. Malinowski, *Factor Analysis in Chemistry*, 2 ed., Wiley, New York **1991**.
- [29] M. J. Frisch, G. W. Trucks, H. B. Schlegel, G. E. Scuseria, M. A. Robb, J. R. Cheeseman, G. Scalmani, V. Barone, G. A. Petersson, H. Nakatsuji, X. Li, M. Caricato, A. V. Marenich, J. Bloino, B. G. Janesko, R. Gomperts, B. Mennucci, H. P. Hratchian, J. V. Ortiz, A. F. Izmaylov, J. L. Sonnenberg, D. Williams-Young, F. Ding, F. Lipparini, F. Egidi, J. Goings, B. Peng, A. Petrone, T. Henderson, D. Ranasinghe, V. G. Zakrzewski, J. Gao, N. Rega, G. Zheng, W. Liang, M. Hada, M. Ehara, K. Toyota, R. Fukuda, J. Hasegawa, M. Ishida, T. Nakajima, Y. Honda, O. Kitao, H. Nakai, T. Vreven, K. Throssell, J. A. Montgomery Jr., J. E. Peralta, F. Ogliaro, M. J. Bearpark, J. J. Heyd, E. N. Brothers, K. N. Kudin, V. N. Staroverov, T. A. Keith, R. Kobayashi, J. Normand, K. Raghavachari, A. P. Rendell, J. C. Burant, S. S. Iyengar, J. Tomasi, M. Cossi, J. M. Millam, M. Klene, C. Adamo, R. Cammi, J. W. Ochterski, R. L. Martin, K. Morokuma, O. Farkas, J. B. Foresman, D. J. Fox, Gaussian 16, Gaussian, Inc., Wallingford, CT **2016**.
- [30] A. Becke, *Phys. Rev. A* **1988**, 38, 3098–3100.
- [31] J. Wang, P. Cieplak, P. A. Kollman, *J. Comput. Chem.* **2000**, 21, 1049–1074.
- [32] D. A. Pearlman, D. A. Case, J. W. Caldwell, W. S. Ross, T. E. Cheatham, S. Debolt, D. M. Ferguson, G. Seibel, P. A. Kollman, *Comp. Phys. Commun.* **1995**, 91, 1–41.
- [33] N. Kamiya, Y. S. Watanabe, S. Ono, J. Higo, *Chem. Phys. Lett.* **2005**, 401, 312–317.
- [34] a) P. Bouř, T. A. Keiderling, *J. Chem. Phys.* **2002**, 117, 4126–4132; b) J. Hudecová, K. H. Hopmann, P. Bouř, *J. Phys. Chem. B* **2012**, 116, 336–342.
- [35] P. Bouř, Qgrad, Academy of Sciences, Prague **2006**.

Manuscript received: May 9, 2023  
Revised manuscript received: June 7, 2023  
Accepted manuscript online: June 7, 2023